ACS central science

http://pubs.acs.org/journal/acscii

Research Article

Induced Ferromagnetic Order of Graphdiyne Semiconductors by Introducing a Heteroatom

Mingjia Zhang,[▽] Xiaoxiong Wang,[▽] Huijuan Sun,[▽] Naiyin Wang, Jianjiang He, Ning Wang, Yunze Long, Changshui Huang,* and Yuliang Li*

Cite This: *ACS Cent. Sci.* 2020, 6, 950–958

Read Online

ACCESS | Metrics & More | Article Recommendations | Supporting Information

ABSTRACT: To date, the realization of ferromagnetism in two-dimensional carbon semiconductors containing only sp electrons has remained a challenge for spintronics. Here, we utilize the atomic-level functionalization strategy to obtain three carbon matrix materials by accurately introducing different light elements (H, F, Cl) into graphdiyne's benzene ring. Their magnetic and conductive characteristics are thoroughly clarified via physical property measurements and DFT calculations. All of these carbon matrix materials retain their excellent intrinsic semiconductor properties. In particular, compared with the paramagnetism of HsGDY and ClsGDY, a robust ferromagnetic ordering as well as high mobility of up to 320 $cm^2\ V^{-1}\ s^{-1}$ was observed in FsGDY, successfully realizing a ferromagnetic semiconductor. Through theory calculations, this unique ferromagnetic coupling can be attributed to the most striking charge transfer between carbon and fluorine atoms, demonstrating the advantages of controllable fabrication. These results not only reveal the important role of atomic-scale doping/substitution in optimizing graphdiyne material but also create new possibilities for manipulating spins and charges in 2D carbon materials.

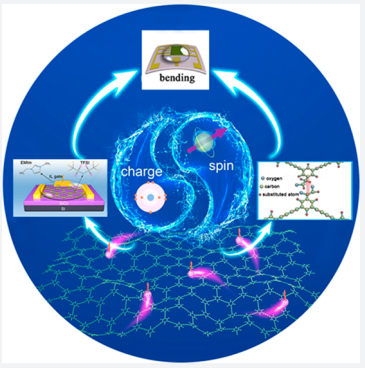

Ferromagnetic integration of semiconductor materials is a research hotspot in the field of materials science, and it provides an effective way for the preparation of new functional devices involving spins such as communication and information processing devices.[1] Among the reported dilute magnetic semiconductors,[2−5] two-dimensional (2D) materials are considered a promising functional material because of their special structure and electronic properties.[6] In particular, carbon-based 2D materials represented by graphene, which contains only s/p electrons, have a long spin lifetime[7,8] and weak spin−orbital interaction,[9] indicating attractive prospects in organic magnets[10] and spintronics.[11] However, practical applications require simultaneous manipulation of semiconductor and magnetic properties.[12] Obtaining graphene-based magnetic semiconductors by electric field control or edge modification has led to various additional efforts to achieve the band gap opening in graphene. Compared with graphene, graphdiyne (GDY), a rapidly developing 2D carbon material,[13] has emerged as one of the most promising candidates for carbon electronic devices[14,15] due to its inherent direct band gap,[16−18] high mobility,[19] and simple preparation methods.[20] The unique structural characteristics of graphdiyne make it easy to be chemically modified, which endows it the possibility to induce magnetic order. Early studies have shown that graphdiyne demonstrates significant paramagnetic characteristics.[21,22] These indicate that if graphdiyne materials can be given ferromagnetic order, the application potential of 2D carbon materials in the semiconductor field can be expanded.

Chemical modification[23] and material design[24] have long been considered to be effective approaches to introduce a ferromagnetic order. Although chemical element doping including nitrogen,[25] sulfur,[26] or ferrum[27] can introduce local magnetic moments to achieve ferromagnetism in 2D materials, it also leads to the suppression of semiconductivity, such as through the band gap reduction. A fluorination strategy has recently been demonstrated to possess a unique influence on the intrinsic properties of 2D materials, which can lead to simultaneously improved magnetic[28] and carrier transport properties.[29] Taking fluorinated graphene as an example, not only have experimental pieces of evidence of colossal negative magnetoresistance[30] and spin-flip scattering[31] been discovered, but it has also been shown to display higher stability and wide-gap semiconducting characteristics,[32] demonstrating the great application potential of fluorination in preparing functionalized carbon materials. Fluorination even converts an electrically insulated h-BN to a magnetic semiconductor combining room-temperature ferromagnetism and improved charge distribution.[33] However, we have to recognize that traditional fluorination methods have shortcomings. For example, fluorine

Received: March 25, 2020
Published: May 13, 2020

https://dx.doi.org/10.1021/acscentsci.0c00348
ACS Cent. Sci. 2020, 6, 950–958

atoms adsorbed on the carbon matrix tend to form clusters, so that each F atom contributes only 1/1000th of a Bohr magneton,[34] which severely limits the introduction of local magnetic moments. Similarly, inhomogeneity also exists despite the fact that wet chemistry-based fluorine dopings can introduce magnetic centers.[35] It is equally crucial for carbon material semiconductors to acquire means to achieve ferromagnetism through chemical modification, while retaining their structure and energy band characteristics. Benefiting from the unique coupling preparation method of graphdiyne, we have conceived an atomic-scale uniformly doping/substitution method using a monomer design strategy, which has been reported in our previous study,[36−38] providing an ideal candidate for exploring ferromagnetic graphdiyne. Moreover, revealing the explicit difference between various doping elements on the intrinsic magnetic properties of graphdiyne is also critical to its potential applications in nanoelectronic devices.

In this study, we present a series of 2D carbon materials with magnetic semiconductor properties, i.e., uniformly distributed heteroatom-modified graphdiyne, including H-substituted, F-substituted, and Cl-substituted graphdiyne (HsGDY, FsGDY, and ClsGDY) films. By strictly controlling the identical synthetic strategy and only altering the precursor's structure, we created an atom-level doped graphdiyne-based carbon material to deeply explore the influence of H, F, and Cl elements on its intrinsic magnetic and electronic properties. Unlike the paramagnetism in HsGDY and ClsGDY, a robust ferromagnetic order in FsGDY below 16 K has been successfully observed due to the unique electronegativity of fluorine, exhibiting a distinct influence of heteroatom modification. Spin-polarized DFT calculations illustrate that the magnetic order of FsGDY is closely related to the enhanced charge transfer compared with HsGDY and ClsGDY, which is further confirmed by electronic transport measurements. These results indicate that selective chemical modification based on element features could enable a ferromagnetic semiconductor and provide guidance for magnetic modulations in 2D carbon materials. On this basis, we utilized the FsGDY film to assemble a high-performance thin-film FET device with a mobility of up to 320 $cm^2 V^{-1} s^{-1}$, which allows the coexistence of spin and charge in 2D carbon materials with a simple self-assembly strategy.

RESULTS AND DISCUSSION

Hydrogen-, fluorine-, and chlorine-modified graphdiynes (hereinafter to be referred as HsGDY, FsGDY, and ClsGDY, respectively) were obtained by a facile strategy to attain precise atomic doping, which is depicted schematically on Figure 1. During the synthesis, the reaction conditions are controlled to be consistent so as to reduce the influence of defects or disorders generated under different conditions on the graphdiyne structure and properties. The critical step in the synthesis process is the preparation of reactive precursors, and the specific synthetic route for these three materials is portrayed in Figure S1. Typical structural schematics and formulas are demonstrated in Figure S2, respectively, showing that the substituted atoms have different electronegativities and atomic radii. After etching the copper, we found that all of these films demonstrate good film-forming properties, as the corresponding optical photographs show in the insets.

Figure 2a−c shows the structural characterizations including Raman and XPS of HsGDY, FsGDY, and ClsGDY,

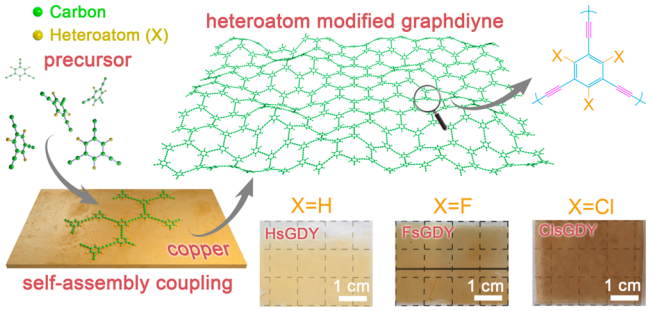

Figure 1. Sketched synthetic route of HsGDY, FsGDY, and ClsGDY. Insets are optical photographs of corresponding films after etching copper foil.

respectively. The Raman spectra of HsGDY, FsGDY, and ClsGDY all show the characteristic peaks at 1360, 1567, and 2162 cm^{-1}, corresponding to structural defects, vibrational modes, and acetylenic linkages (—C≡C—C≡C—).[39] Here, the relative intensities of D and G peaks are used to characterize the content of defects.[40] For our three samples, the I_D/I_G ratios are all around 0.7, indicating that there are a relatively small number of defects. Moreover, the change of I_D/I_G ratio with doped elements is not obvious, suggesting that the amount of defects in different samples is not much different. The overall chemical composition of these samples characterized by X-ray photoelectron spectroscopy (XPS) can be used to determine the bonding situation and average element contents including carbon and other introduced elements (Figure S3). The existence of the O 1s peak may be attributed to the absorbed air in the porous carbon network[41] as well as the possible oxidation of the terminal alkyne in graphdiyne. In particular, an obvious F 2p peak and Cl 2p peak are observed for FsGDY and ClsGDY, respectively (Figure 2b), suggesting the efficient introduction of fluorine or chlorine into graphdiyne. Figure 2c shows a high-resolution C 1s spectrum of HsGDY, which can be resolved into four characteristic peaks representing C≡C (sp), C—C (sp^2), C—O, and C═O bonds.[42] For FsGDY and ClsGDY, besides these four essential peaks, another characteristic peak attributed to the C—F bond (286.1 eV) and C—Cl (286.3 eV) bond can be simulated, confirming the introduction of fluorine and chlorine atoms. To further identify the electronic structure and local atomic arrangements of the heteroatom-modified graphdiyne, synchrotron radiation XANES (X-ray absorption near edge structure) measurements were performed. Figure 2d,e demonstrates the C K-edge XANES spectra of HsGDY and FsGDY, and three main characteristic peaks can be assigned to the π^* excitation of aromatic carbon−carbon bonds, the π^* excitation of C≡C bonds, and the σ^* excitation of carbon—carbon bonds, respectively.[43] For HsGDY, a remarkable feature at 288.89 eV can be attributed to the sp^3 hybridized states arising from oxygenated functional groups such as carboxylate,[43] and the covered peak at 287.5 eV can be assigned to C—H resonance.[44] For FsGDY, besides the oxygenated functional resonance, another signature peak of C═C—F is observed. Meanwhile, the fluorine spectrum shown in the inset of Figure 2e also confirms the presence of a C—F bond,[45] indicating the effective fluorination on the benzene ring.

As for the morphology features of HsGDY, FsGDY, and ClsGDY, scanning electron microscopy (SEM) images can be used to verify the uniform surface with slightly different

https://dx.doi.org/10.1021/acscentsci.0c00348
ACS Cent. Sci. 2020, 6, 950−958

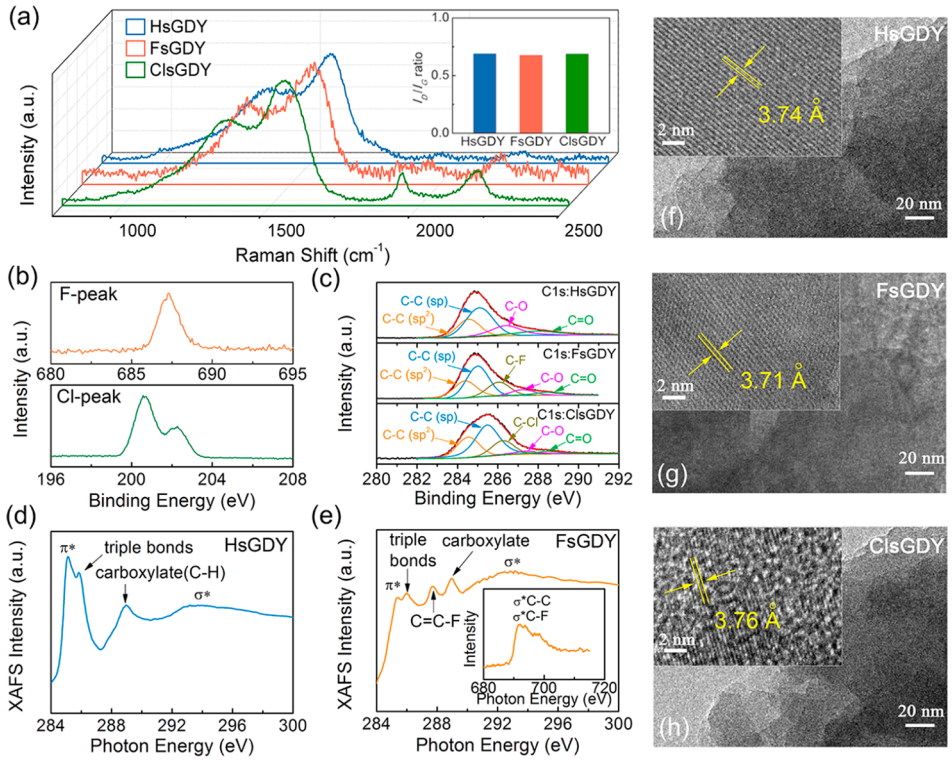

Figure 2. (a) Raman spectra of HsGDY, FsGDY, and ClsGDY. Inset is the I_D/I_G ratio. (b) Fluorine peak of FsGDY and chlorine peak of ClsGDY measured in XPS spectra. (c) High-resolution C 1s XPS spectra of HsGDY, FsGDY, and ClsGDY. (d) C K-edge XANES spectrum of HsGDY. (e) C K-edge XANES spectrum of FsGDY. Inset is the F K-edge XANES spectrum. TEM and high-resolution TEM images of HsGDY (f), FsGDY (g), and ClsGDY (h).

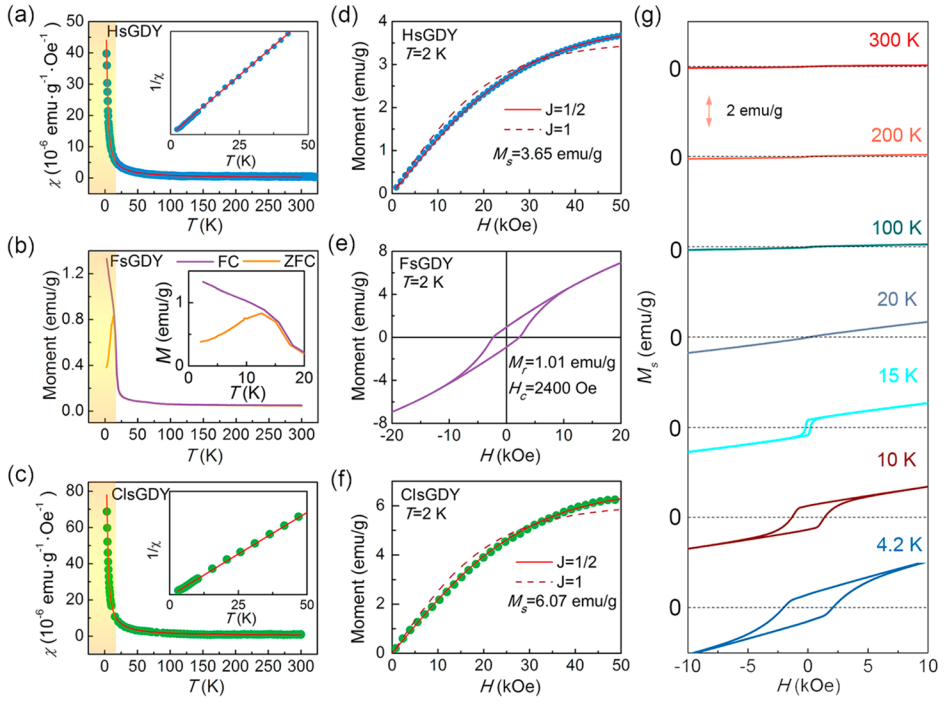

Figure 3. Typical $\chi-T$ curves of HsGDY (a), FsGDY (b), and ClsGDY (c) with the applied magnetic field H = 2000 Oe. Red lines correspond to the fitting by Curie law. The $M-T$ curves of FsGDY are measured by zero-field cooling (ZFC) and field cooling (FC), respectively. $M-H$ curves of HsGDY (d), FsGDY (e), and ClsGDY (f) measured at 2 K, respectively. The solid and dashed lines are Brillouin fits to the paramagnetic magnetization curves with J = 1/2 and J = 1, respectively. (g) Hysteresis loops of the FsGDY sample measured at various temperatures.

textures (Figure S4). Subsequent elemental analysis indicated that carbon and doped fluorine and chlorine atoms are uniformly distributed (Figures S5−S8). High-resolution SEM images are used to evaluate the different agglomerate states

https://dx.doi.org/10.1021/acscentsci.0c00348
ACS Cent. Sci. 2020, 6, 950−958

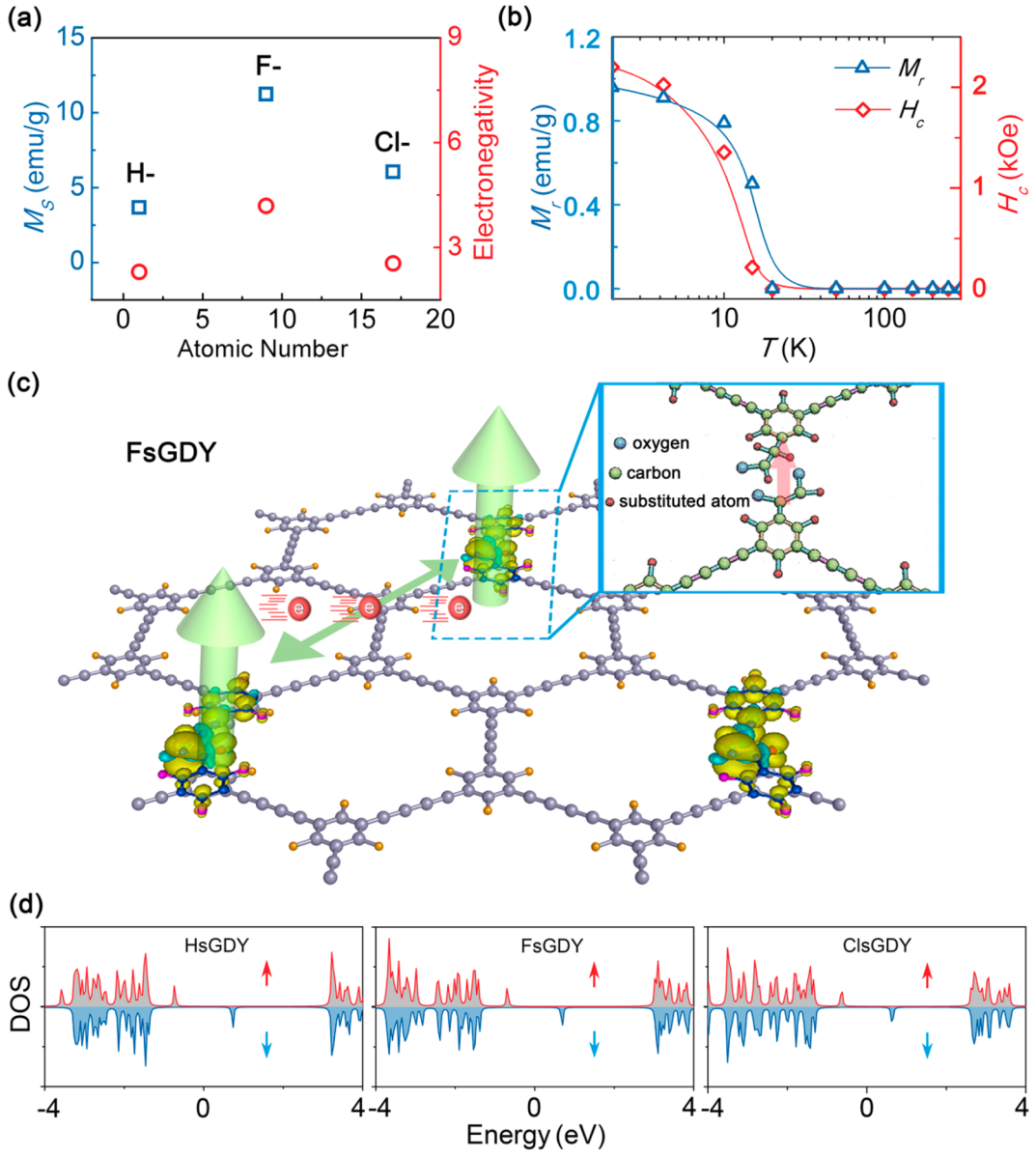

Figure 4. (a) Variation of M_s and electronegativity in graphdiyne substituted by different elements. (b) Temperature dependence of the coercivity H_c and the remanent magnetization M_r. (c) DFT simulation model and calculated electronic cloud distribution for FsGDY, showing the origin of ferromagnetism. (d) Corresponding spin-resolved DOS of HsGDY, FsGDY, and ClsGDY with oxygenated functional groups.

(Figures S9−S11): for HsGDY and ClsGDY, the particles tend to form a textured microstructure with obvious polyporous characteristics, while for FsGDY the particles are easy to reunite to form a denser morphology due to the cluster characteristics of F atoms among different flakes. The transmission electron microscopy (TEM) images shown in Figure 2f−h are used to further demonstrate the continuous and uniform microstructures with layered stacking features for all of these three materials. Using high-resolution transmission electron microscopy (HRTEM) as shown in the corresponding illustrations, we found that the corresponding interlayer spacings for HsGDY, FsGDY, and ClsGDY are 3.74, 3.71, and 3.76 Å, respectively, which is marked by arrows.[46] A small difference in spacing indicates that the layered structural characteristics have not changed significantly with different element modification, because the synthetic routes of these three materials are similar except the different reaction monomer.

For investigating the magnetic properties of the chemical-substituted graphdiyne, the magnetization characteristics of those materials measured with different temperatures ranging from 300 to 2 K are shown in Figure 3. From the temperature dependence of magnetic susceptibility ($\chi-T$) curves (Figure 3a−c), we can see that both the HsGDY and ClsGDY display the typical paramagnetic properties in the whole temperature range, which can be well described by the Curie law. For FsGDY, a typical bifurcation between the field cooled (FC) magnetization and zero field cooled (ZFC) magnetization can be observed below 16 K, suggesting the appearance of ferromagnetic order. In order to obtain quantitative magnetic moment characteristics, we also measured the magnetization curves at 2 K, which is shown in Figure 3d−f. For HsGDY and ClsGDY, as the magnetic field increases, the magnetization increases quickly and eventually tends to saturate because of the arrangement of almost all spins along the orientation of the magnetic field, verifying the paramagnetic properties. Herein

https://dx.doi.org/10.1021/acscentsci.0c00348
ACS Cent. Sci. 2020, 6, 950−958

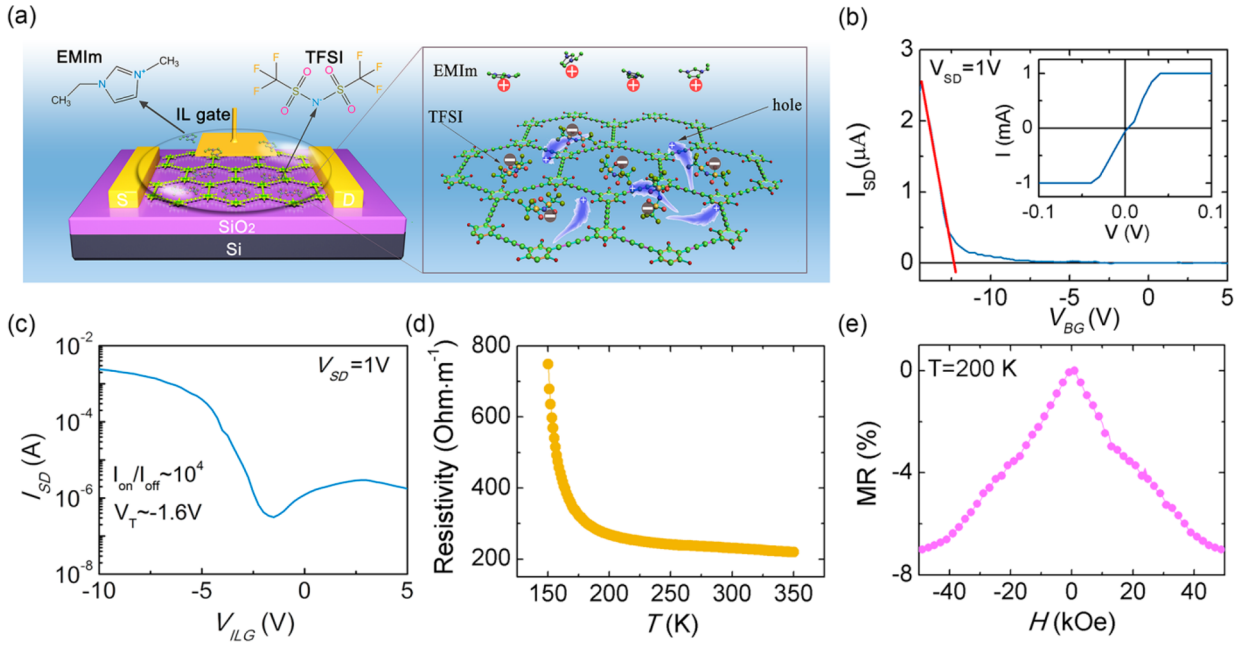

Figure 5. (a) Schematic diagram of the flexible FET device based on FsGDY film using ionic liquid as the gate. Transfer curves of FsGDY FET fabricated on SiO_2/Si substrate with (b) SiO_2 as gate and (c) ionic liquid as gate, respectively. (d) Temperature-dependent resistivity curve of flexible FsGDY. (e) Magnetoresistance of flexible FsGDY measured at 200 K.

the variation of magnetization can be accurately described by the Brillouin function as follows:[47]

$$M = M_s\left[\frac{2J+1}{2J}\,\mathrm{cont}\left(\frac{2J+1}{2J}x\right) - \frac{1}{2J}\,\mathrm{cont}\left(\frac{x}{2J}\right)\right],\quad x = gJ\mu_B H/k_B T,$$

where M_s is the saturation magnetization, μ_B is the Bohr magneton, k_B is the Boltzmann constant, g is the g-factor, and J is the angular momentum quantum number. As shown by solid red lines, both the experimental data of HsGDY and ClsGDY can be fitted better using $g = 2$, $J = 1/2$ compared with that using $g = 2$, $J = 1$, suggesting that the magnetism originates from the electronic magnetic moment without any coupling effect between different spins. Besides, the obtained M_s values of HsGDY and ClsGDY measured at 2 K are 3.67 and 6.06 emu/g, respectively, which is almost an order of magnitude higher than the value of pristine graphdiyne (Table S1),[21] indicating that chemical modification on the benzene ring of graphdiyne can be used as an effective method to introduce local magnetic moments. As for FsGDY, a typical ferromagnetic hysteresis can be observed, and the remanent magnetization M_r as well as coercive field H_c are 1.01 emu/g and 2400 Oe, respectively, which is much higher than that obtained in doped graphene or even diluted magnetic semiconductors, suggesting a robust ferromagnetic spin ordering with strong remanence retention characteristics (Figure S12) as well as the potential application in carbon-based magnets. On this basis, we further measured the magnetization curve of FsGDY in detail, which is shown in Figure 3g. For $T < T_c$, with the decrease of temperature, the ferromagnetic hysteresis increases gradually, which results in the enhancement of both M_r and H_c. As for $T > T_c$, the magnetization curve displays a monotonous increase with the magnetic field; in particular, at high temperature the $M-H$ curve demonstrates a linear dependence of applied magnetic field, further confirming the paramagnetic characteristic above T_c.

In order to further clarify the regulation of graphdiyne's magnetic properties by a molecular design strategy, we compared the saturation magnetic moments of three samples with the electronegativity of the corresponding modified elements, as presented in Figure 4a. It is obvious that the saturation magnetic moment is closely related to the electronegativity of the particular element. This is mainly due to the fact the enhancement of the electronegativity of the modified element in carbon materials can introduce an enhanced local magnetic moment,[37] which confirms that the fluorine element is beneficial to inducing ferromagnetism in graphdiyne. Next, we extracted the temperature-dependent M_r and H_c values from magnetization curves, as Figure 4b delineated, and found that both the M_r and H_c show a sharp increase with decreasing temperatures, further verifying the robust ferromagnetic ordering.

To gain insight into the origin of magnetic order in heteroatom-substituted graphdiyne, spin-polarized density functional theoretical calculations were performed. Taking FsGDY as an example, the calculation results with an idealized defect-free unit cell indicate an intrinsic band gap of 2 eV; meanwhile no local magnetism can be obtained from the symmetric DOS diagram (Figure S13). If even a single monomer is missing during the film formation process, the local magnetic moment would not be introduced further (Figure S14). Thus, in this condition we must consider the contribution of the lattice defect such as terminal alkyne oxidation, which is demonstrated in the previous report[37] and has also been revealed in the XPS and XANES measurement mentioned above. The electron cloud distribution represented by FsGDY is shown in Figure 4c, while the electronic cloud distribution of the other two materials can be found in the Supporting Information (Figures S15 and S16). All the calculated DOS results shown in Figure 4d display unsymmetrical spin-up and spin-down states, suggesting that an indisputable local magnetic moment is induced in the heteroatom-substituted graphdiyne. The calculated local magnetic moment value of each unit cell using the simulation

https://dx.doi.org/10.1021/acscentsci.0c00348
ACS Cent. Sci. 2020, 6, 950−958

model pictured in Figure 4c is about 1 μ_B, proving the importance of oxygenated functional groups in inducing local magnetic moments. The spin-polarized electron cloud distributions indicate a significant charge transfer on the alkyne chain. Based on Bader charge analysis, we can obtain the charge transfer among the heteroatom and C atoms, as summarized in Table S2. Compared with the results of the nondefective model, the electron transfer number does not change much after considering the defects, especially for FsGDY, revealing the dominant role of doping in electron transfer. On the other hand, the influence of different doped elements on electron transfer number varies significantly, and fluorine modification can lead to the most charge transfer (0.62 e), promoting a significantly enhanced carrier transport throughout the whole carbon matrix. As for the influence of the defect, it mainly contributes to the induced local magnetic moment. Thus, on the intrinsic paramagnetic background, the spins easily form ferromagnetic couplings by a Ruderman−Kittel−Kasuya−Yosida (RKKY)-like[14] interaction through conduction electrons, which is similar to that reported in graphene,[48,49] resulting in the appearance of long-range ferromagnetic ordering.[50] Besides, to clarify the influence of different elements on the intrinsic electromagnetic properties of graphdiyne, the same calculations for oxygenated GDY and bromine-substituted GDY (BrsGDY) are also performed (Figures S17 and S18). Though the calculated local magnetic moments and DOS are similar to that of our synthesized substituted graphdiyne, the charge transfer caused by the carboxylate or Br atom is still much inferior to that in FsGDY (Table S2). Hereby, we can not only confirm that the long-range magnetic order in this kind of material system originates from the RKKY-like interaction but also reveal the uniqueness of fluorine modification; that is, the optimized conductivity enhances the probability of coupling through conduction electrons. These results provide strategies for subsequent optimization of such 2D carbon materials.

Inspired by the unique influence of the fluorine atoms on band structure and charge transfer of graphdiyne in theory, we further investigated the semiconducting properties of FsGDY based on a UV−vis absorption spectrum and conductivity measurement. Given the improved electrical properties of atomic-scale fluorine-substituted graphdiyne films, we can design a series of different devices, namely, flexible devices, and the schematic structure is schematically illustrated in Figure 5a. When using SiO_2(300 nm)/Si substrates, we fabricated the back-gated FsGDY field-effect transistor (FET) after transferring pristine films (Figure S19). The UV−vis absorption spectrum of the raw FsGDY film used in FET fabrication (Figure S20) demonstrates the absence of exciton peaks, indicating uniform introduction of light element due to the special monomer design strategy, which is different from the inhomogeneities introduced by wet chemical doping. The calculated element-dependent energy band gap via the Kubelka−Munk transformation[51−53] demonstrates a band gap of 1.54 eV for FsGDY. Compared with the band gap of HsGDY and ClsGDY (Figure S20), FsGDY has the highest band gap value, which is beneficial for semiconductor devices based on wide band gaps. On the other hand, all these materials still maintain a moderate band gap greater than 1 eV, eliminating the band gap suppression caused by conventional chemical doping in graphdiyne materials.[54] Conjointly, the measured conductive $I-V$ curve of FsGDY on the copper sheet is also plotted in Figure 5b, and we can henceforth obtain the conductivity value as 6.10×10^{-3} S m^{-1}. For HsGDY and ClsGDY, the conductivity values are 0.89×10^{-3} and 1.97×10^{-3} S m^{-1} (Figure S21), verifying the significant modification by fluorine for carrier transport in graphdiyne. Based on the transfer curve of FsGDY FET shown in Figure 5b, an FsGDY mobility of up to 320 cm^2 V^{-1} s^{-2} can be obtained. We subsequently adopted the high-capacitance ionic liquid 1-ethyl-3-methylimidazolium bis(trifluoromethylsulfonyl)imide (EMIm TFSI) as the top dielectric layer to more effectively induce carriers in the channel layer. As displayed in Figure 5a, the FsGDY structure has larger pores compared with the pristine graphdiyne, rendering the ion dielectric layer's modulation easy to implement. After applying the source-drain voltage V_{sd} = 1 V and after a short period of stabilization (Figure S22), we obtained a transfer curve as shown in Figure 5c. The measured on-state current I_{on} and switch ratio I_{on}/I_{off} values were 2.4 mA and nearly 10^4, respectively, demonstrating a remarkable application potential in practical transistors compared with the traditional graphdiyne FET devices.

Considering the widespread application of functionalized graphdiyne,[55−57] we also designed a flexible electronic prototype device based on FsGDY films. Using a flexible PET substrate, we assembled a bendable magnetoresistive prototype device, as depicted in the left of Figure S23. This device's temperature-dependent resistivity is revealed in Figure 5d, and more convincing pieces of evidence of the semiconductor nature of FsGDY can be given by the increased resistivity with decreasing temperatures. Albeit the ionic liquid is covered on this device (as shown in Figure S23), a flexible transistor having excellent transfer characteristics can still be obtained (Figure S24). More importantly, the magnetotransport measurement performed at 200 K exhibits a negative magnetoresistance (MR) of approximately −8%, as pictured in Figure 5e, indicating the existence of local magnetic moments. When a magnetic field is applied, more spins are aligned, and thus, the spin scattering is reduced, eventually resulting in the decrease of resistance.[58] Compared with conventional ferromagnetic materials, the structural flexibility of FsGDY enables its use in wearable devices. Up to now, the promising application of such a ferromagnetic semiconductor in future multifunctional or spintronic devices makes us verify the important role of precise chemical modification in physical property control of graphdiyne, which may open up a novel method to design 2D functional materials.

CONCLUSION

To conclude, we have developed a precursor predesigned strategy to prepare precise hydrogen-, fluorine-, and chlorine-substituted graphdiyne-based nanocarbon materials. Characterizations of structure and morphology have shown that the HsGDY, FsGDY, and ClsGDY are well obtained with sp and sp^2 hybridization carbon and substituted light atoms homogeneously distributed. Considerable magnetic ordering and enhanced carrier transport properties have been confirmed in both experiments and spin-polarized theory calculations, which shows a close correlation with electronegativity. Among those materials, FsGDY exhibits robust ferromagnetism and a high mobility of up to 320 cm^2 V^{-1} s^{-1}, hence achieving the coexistence of ferromagnetism and semiconductivity. Taking advantage of the exceptional film-forming and electromagnetic properties in FsGDY film, we also fabricated a flexible prototype device and realized a negative magnetoresistance effect of 8%. Considering the accurate, low-cost, and feasible

https://dx.doi.org/10.1021/acscentsci.0c00348
ACS Cent. Sci. 2020, 6, 950−958

elements modification strategies and device fabrication nanotechnologies, we expect the future application of those 2D carbon materials to be in spintronics such as magnetoresistive random access memory and magnetic switching.

METHODS

Synthesis of Chemically Modified Graphdiyne. The molecular self-assembly methods on pure copper substrate with special precursor design are used to achieve precise doping of graphdiyne. HsGDY and ClsGDY films were prepared by synthesizing two different precursors (the raw materials are the commercial tribromophenyl and 1,3,5-trichlorobenzene, respectively) and then the coupling reaction on the surface of the copper sheet according to the previous study,[39] as sketched in Figure 1a. To synthesize FsGDY, we use 1,3,5-trifluorobenzene as the initial raw material to obtain the reactive precursor by bromination with bromine. A large-area FsGDY film on the copper foil was realized by a coupling reaction with reference to the polymerization process of HsGDY and ClsGDY. Then, the large-area HsGDY, ClsGDY, and FsGDY films were severally collected by a series of treatments including corroding copper with the newly prepared hydrochloric acid, purifying with deionized water and acetone, and vacuum desiccation. The above process of copper removal and cleaning is repeated several times in a clean environment to exclude metal or magnetic impurities. The collected membrane flakes were carefully ground into uniform powders in an agate mortar to facilitate the magnetic measurement. All sample masses were accurately weighed using high-precision electronic balances with 0.01 mg resolution.

Fabrication of the FsGDY Transistor and Flexible Devices. The raw FsGDY film grown on copper foil was placed in a newly prepared hydrochloric acid solution to etch away copper. Subsequently, the film was transferred to ultrapure water and then transferred onto the SiO_2/Si substrate, which demonstrates an average thickness of 750 nm (Figure S25). Ag electrodes were deposited with a metallic shadow mask to fabricate the back-gated Ag/F-GDY/SiO_2/Si FET device. A droplet of ion liquid was dropped onto the film surface, and one of the Ag electrodes was used as the ionic liquid gate. For the flexible FsGDY prototype device, we (i) first deposited the interdigital Ag electrode on the PET substrate, and (ii) then transferred a piece of FsGDY film onto the substrate. (iii) After the FsGDY film is dried, we coated the ionic liquid dielectric layer as the gate.

Characterization and Measurement. The structural features of Hs-, Fs-, and ClsGDY were analyzed by using Raman spectra (NT-MDT NTEGRA Spectra system). The X-ray photoelectron spectrometer (XPS, ULVAC-PHI) was carried out to investigate the specific chemical component and bonding environment. Morphological characteristics were measured using a scanning electron microscope (Hitachi S-4800 FESEM). Magnetization characteristics were measured by a vibrating sample magnetometer (PPMS VSM, Quantum Design) in the temperature range from 2 to 300 K. $I-V$ and transistor measurements were carried out by using a semiconductor parameter analyzer (Keithley 4200 SC) at room temperature. The mobility μ is calculated according to the following formula: $\mu = [dI/dV_g]\cdot[L/(WC_gV_{ds})]$.[59] As for the electrical resistance and magnetoresistance properties of the flexible FsGDY film, they are measured using the transport component of the physical property measurement system (PPMS, Quantum Design).

First-Principles Calculations. Spin-polarized DFT calculations were performed using the Vienna ab initio simulation package (VASP). Electron−nuclear interactions were described by the projector augmented wave (PAW) method. The Perdew−Burke−Ernzerhof (PBE) function was used to describe the exchange-correlation energy. The plane-wave cutoff was set to 500 eV, and the geometries were optimized with all forces less than 0.01 eV $Å^{-1}$. Different types of structural models were constructed with experimental information.

ASSOCIATED CONTENT

Supporting Information

The Supporting Information is available free of charge at https://pubs.acs.org/doi/10.1021/acscentsci.0c00348.

Additional figures regarding the specific synthetic route, SEM, EDS, DFT calculation, UV−vis absorption spectra, device test configuration, and physical properties (PDF)

AUTHOR INFORMATION

Corresponding Authors

Changshui Huang − *Qingdao Institute of Bioenergy and Bioprocess Technology, Chinese Academy of Sciences, Qingdao 266101, P. R. China; Center of Materials Science and Optoelectronics Engineering, University of Chinese Academy of Sciences, Beijing 100049, P. R. China;* orcid.org/0000-0001-5169-0855; Email: huangcs@qibebt.ac.cn

Yuliang Li − *Beijing National Laboratory for Molecular Sciences (BNLMS), CAS Key Laboratory of Organic Solids, Institute of Chemistry, Chinese Academy of Sciences, Beijing 100190, P. R. China;* orcid.org/0000-0001-5279-0399; Email: ylli@iccas.ac.cn

Authors

Mingjia Zhang − *Qingdao Institute of Bioenergy and Bioprocess Technology, Chinese Academy of Sciences, Qingdao 266101, P. R. China*

Xiaoxiong Wang − *College of Physics, Qingdao University, Qingdao 266071, P. R. China*

Huijuan Sun − *College of Physics, Qingdao University, Qingdao 266071, P. R. China;* orcid.org/0000-0003-0442-4161

Naiyin Wang − *Department of Electronic Materials Engineering, Research School of Physics, The Australian National University, Canberra, Australian Capital Territory 2601, Australia;* orcid.org/0000-0001-5788-9187

Jianjiang He − *Qingdao Institute of Bioenergy and Bioprocess Technology, Chinese Academy of Sciences, Qingdao 266101, P. R. China*

Ning Wang − *School of Chemistry and Chemical Engineering, Shandong University, Jinan 250100, P. R. China*

Yunze Long − *College of Physics, Qingdao University, Qingdao 266071, P. R. China;* orcid.org/0000-0002-4278-4515

Complete contact information is available at: https://pubs.acs.org/10.1021/acscentsci.0c00348

Author Contributions

[▽]M.Z., X.W., and H.S. contributed equally. The manuscript was written through contributions of all authors. All authors have given approval to the final version of the manuscript.

https://dx.doi.org/10.1021/acscentsci.0c00348
ACS Cent. Sci. 2020, 6, 950−958

Notes

The authors declare no competing financial interest.

■ ACKNOWLEDGMENTS

This study was supported by the National Natural Science Foundation of China (51802324, 21790050, 21790051, 51822208, 21771187), the Frontier Science Research Project (QYZDB-SSW-JSC052) of the Chinese Academy of Sciences, and the Taishan Scholars Program of Shandong Province (tsqn201812111).

■ REFERENCES

(1) Wang, Z.; Zhang, T.; Ding, M.; Dong, B.; Li, Y.; Chen, M.; Li, X.; Huang, J.; Wang, H.; Zhao, X.; Li, Y.; Li, D.; Jia, C.; Sun, L.; Guo, H.; Ye, Y.; Sun, D.; Chen, Y.; Yang, T.; Zhang, J.; Ono, S.; Han, Z.; Zhang, Z. Electric-field control of magnetism in a few-layered van der Waals ferromagnetic semiconductor. *Nat. Nanotechnol.* **2018**, *13*, 554−559.

(2) Yang, J.; Fainblat, R.; Kwon, S. G.; Muckel, F.; Yu, J. H.; Terlinden, H.; Kim, B. H.; Iavarone, D.; Choi, M. K.; Kim, I. Y.; Park, I.; Hong, H.-K.; Lee, J.; Son, J. S.; Lee, Z.; Kang, K.; Hwang, S.-J.; Bacher, G.; Hyeon, T. Route to the Smallest Doped Semiconductor: Mn2+-Doped (CdSe)13 Clusters. *J. Am. Chem. Soc.* **2015**, *137*, 12776−12779.

(3) Dietl, T. A ten-year perspective on dilute magnetic semiconductors and oxides. *Nat. Mater.* **2010**, *9*, 965.

(4) Huang, C.; Feng, J.; Wu, F.; Ahmed, D.; Huang, B.; Xiang, H.; Deng, K.; Kan, E. Toward Intrinsic Room-Temperature Ferromagnetism in Two-Dimensional Semiconductors. *J. Am. Chem. Soc.* **2018**, *140*, 11519−11525.

(5) Yang, S.; Li, W.; Ye, C.; Wang, G.; Tian, H.; Zhu, C.; He, P.; Ding, G.; Xie, X.; Liu, Y.; Lifshitz, Y.; Lee, S.-T.; Kang, Z.; Jiang, M. C3N—A 2D Crystalline, Hole-Free, Tunable-Narrow-Bandgap Semiconductor with Ferromagnetic Properties. *Adv. Mater.* **2017**, *29*, 1605625.

(6) Liu, H.; Bao, L.; Zhou, Z.; Che, B.; Zhang, R.; Bian, C.; Ma, R.; Wu, L.; Yang, H.; Li, J.; Gu, C.; Shen, C.-M.; Du, S.; Gao, H.-J. Quasi-2D Transport and Weak Antilocalization Effect in Few-layered VSe2. *Nano Lett.* **2019**, *19*, 4551−4559.

(7) Kamalakar, M. V.; Groenveld, C.; Dankert, A.; Dash, S. P. Long distance spin communication in chemical vapour deposited graphene. *Nat. Commun.* **2015**, *6*, 6766.

(8) Yan, W.; Phillips, L. C.; Barbone, M.; Hämäläinen, S. J.; Lombardo, A.; Ghidini, M.; Moya, X.; Maccherozzi, F.; van Dijken, S.; Dhesi, S. S.; Ferrari, A. C.; Mathur, N. D. Long Spin Diffusion Length in Few-Layer Graphene Flakes. *Phys. Rev. Lett.* **2016**, *117*, 147201.

(9) Pesin, D.; MacDonald, A. H. Spintronics and pseudospintronics in graphene and topological insulators. *Nat. Mater.* **2012**, *11*, 409−416.

(10) Tuček, J.; Holá, K.; Bourlinos, A. B.; Błoński, P.; Bakandritsos, A.; Ugolotti, J.; Dubecký, M.; Karlický, F.; Ranc, V.; Čépe, K.; Otyepka, M.; Zbořil, R. Room temperature organic magnets derived from sp3 functionalized graphene. *Nat. Commun.* **2017**, *8*, 14525.

(11) Han, W.; Kawakami, R. K.; Gmitra, M.; Fabian, J. Graphene spintronics. *Nat. Nanotechnol.* **2014**, *9*, 794.

(12) Ando, K. Seeking Room-Temperature Ferromagnetic Semiconductors. *Science* **2006**, *312*, 1883−1885.

(13) Huang, C.; Li, Y.; Wang, N.; Xue, Y.; Zuo, Z.; Liu, H.; Li, Y. Progress in Research into 2D Graphdiyne-Based Materials. *Chem. Rev.* **2018**, *118*, 7744−7803.

(14) Zheng, H.; Li, Y.; Liu, H.; Yin, X.; Li, Y. Construction of heterostructure materials toward functionality. *Chem. Soc. Rev.* **2011**, *40*, 4506−4524.

(15) Gao, X.; Zhu, Y.; Yi, D.; Zhou, J.; Zhang, S.; Yin, C.; Ding, F.; Zhang, S.; Yi, X.; Wang, J.; Tong, L.; Han, Y.; Liu, Z.; Zhang, J. Ultrathin graphdiyne film on graphene through solution-phase van der Waals epitaxy. *Sci. Adv.* **2018**, *4*, No. eaat6378.

(16) Li, Y.; Xu, L.; Liu, H.; Li, Y. Graphdiyne and graphyne: from theoretical predictions to practical construction. *Chem. Soc. Rev.* **2014**, *43*, 2572−86.

(17) Luo, G.; Qian, X.; Liu, H.; Qin, R.; Zhou, J.; Li, L.; Gao, Z.; Wang, E.; Mei, W.-N.; Lu, J.; Li, Y.; Nagase, S. Quasiparticle energies and excitonic effects of the two-dimensional carbon allotrope graphdiyne: Theory and experiment. *Phys. Rev. B: Condens. Matter Mater. Phys.* **2011**, *84*, No. 075439.

(18) Li, Y.; Liu, T.; Liu, H.; Tian, M.-Z.; Li, Y. Self-Assembly of Intramolecular Charge-Transfer Compounds into Functional Molecular Systems. *Acc. Chem. Res.* **2014**, *47*, 1186−1198.

(19) Long, M.; Tang, L.; Wang, D.; Li, Y.; Shuai, Z. Electronic Structure and Carrier Mobility in Graphdiyne Sheet and Nanoribbons: Theoretical Predictions. *ACS Nano* **2011**, *5*, 2593−2600.

(20) Shang, H.; Zuo, Z.; Yu, L.; Wang, F.; He, F.; Li, Y. Low-Temperature Growth of All-Carbon Graphdiyne on a Silicon Anode for High-Performance Lithium-Ion Batteries. *Adv. Mater.* **2018**, *30*, 1801459.

(21) Zhang, M.; Wang, X.; Sun, H.; Wang, N.; Lv, Q.; Cui, W.; Long, Y.; Huang, C. Enhanced paramagnetism of mesoscopic graphdiyne by doping with nitrogen. *Sci. Rep.* **2017**, *7*, 11535.

(22) Zheng, Y.; Chen, Y.; Lin, L.; Sun, Y.; Liu, H.; Li, Y.; Du, Y.; Tang, N. Intrinsic magnetism of graphdiyne. *Appl. Phys. Lett.* **2017**, *111*, No. 033101.

(23) Allouche, F.; Lapadula, G.; Siddiqi, G.; Lukens, W. W.; Maury, O.; Le Guennic, B.; Pointillart, F.; Dreiser, J.; Mougel, V.; Cador, O.; Copéret, C. Magnetic Memory from Site Isolated Dy(III) on Silica Materials. *ACS Cent. Sci.* **2017**, *3*, 244−249.

(24) Gui, X.; Pletikosic, I.; Cao, H.; Tien, H.-J.; Xu, X.; Zhong, R.; Wang, G.; Chang, T.-R.; Jia, S.; Valla, T.; Xie, W.; Cava, R. J. A New Magnetic Topological Quantum Material Candidate by Design. *ACS Cent. Sci.* **2019**, *5*, 900−910.

(25) Błoński, P.; Tuček, J.; Sofer, Z.; Mazánek, V.; Petr, M.; Pumera, M.; Otyepka, M.; Zbořil, R. Doping with Graphitic Nitrogen Triggers Ferromagnetism in Graphene. *J. Am. Chem. Soc.* **2017**, *139*, 3171−3180.

(26) Tucek, J.; Blonski, P.; Sofer, Z.; Simek, P.; Petr, M.; Pumera, M.; Otyepka, M.; Zboril, R. Sulfur Doping Induces Strong Ferromagnetic Ordering in Graphene: Effect of Concentration and Substitution Mechanism. *Adv. Mater.* **2016**, *28*, 5045−53.

(27) Li, B.; Xing, T.; Zhong, M.; Huang, L.; Lei, N.; Zhang, J.; Li, J.; Wei, Z. A two-dimensional Fe-doped SnS2 magnetic semiconductor. *Nat. Commun.* **2017**, *8*, 1958.

(28) Feng, Q.; Tang, N.; Liu, F.; Cao, Q.; Zheng, W.; Ren, W.; Wan, X.; Du, Y. Obtaining High Localized Spin Magnetic Moments by Fluorination of Reduced Graphene Oxide. *ACS Nano* **2013**, *7*, 6729−6734.

(29) Feng, W.; Long, P.; Feng, Y.; Li, Y. Two-Dimensional Fluorinated Graphene: Synthesis, Structures, Properties and Applications. *Adv. Sci.* **2016**, *3*, 1500413.

(30) Hong, X.; Cheng, S. H.; Herding, C.; Zhu, J. Colossal negative magnetoresistance in dilute fluorinated graphene. *Phys. Rev. B: Condens. Matter Mater. Phys.* **2011**, *83*, No. 085410.

(31) Hong, X.; Zou, K.; Wang, B.; Cheng, S. H.; Zhu, J. Evidence for Spin-Flip Scattering and Local Moments in Dilute Fluorinated Graphene. *Phys. Rev. Lett.* **2012**, *108*, 226602.

(32) Robinson, J. T.; Burgess, J. S.; Junkermeier, C. E.; Badescu, S. C.; Reinecke, T. L.; Perkins, F. K.; Zalalutdniov, M. K.; Baldwin, J. W.; Culbertson, J. C.; Sheehan, P. E.; Snow, E. S. Properties of Fluorinated Graphene Films. *Nano Lett.* **2010**, *10*, 3001−3005.

(33) Radhakrishnan, S.; Das, D.; Samanta, A.; de los Reyes, C. A.; Deng, L.; Alemany, L. B.; Weldeghiorghis, T. K.; Khabashesku, V. N.; Kochat, V.; Jin, Z.; Sudeep, P. M.; Martí, A. A.; Chu, C.-W.; Roy, A.; Tiwary, C. S.; Singh, A. K.; Ajayan, P. M. Fluorinated h-BN as a magnetic semiconductor. *Sci. Adv.* **2017**, *3*, No. e1700842.

(34) Nair, R. R.; Sepioni, M.; Tsai, I. L.; Lehtinen, O.; Keinonen, J.; Krasheninnikov, A. V.; Thomson, T.; Geim, A. K.; Grigorieva, I. V. Spin-half paramagnetism in graphene induced by point defects. *Nat. Phys.* **2012**, *8*, 199.

https://dx.doi.org/10.1021/acscentsci.0c00348
ACS Cent. Sci. 2020, 6, 950−958

(35) Radhakrishnan, S.; Das, D.; Deng, L.; Sudeep, P. M.; Colas, G.; los Reyes, C. A.; Yazdi, S.; Chu, C. W.; Martí, A. A.; Tiwary, C. S.; Filleter, T.; Singh, A. K.; Ajayan, P. M. An Insight into the Phase Transformation of WS2 upon Fluorination. *Adv. Mater.* **2018**, *30*, 1803366.
(36) He, J.; Wang, N.; Cui, Z.; Du, H.; Fu, L.; Huang, C.; Yang, Z.; Shen, X.; Yi, Y.; Tu, Z.; Li, Y. Hydrogen substituted graphdiyne as carbon-rich flexible electrode for lithium and sodium ion batteries. *Nat. Commun.* **2017**, *8*, 1172.
(37) He, J.; Wang, N.; Yang, Z.; Shen, X.; Wang, K.; Huang, C.; Yi, Y.; Tu, Z.; Li, Y. Fluoride graphdiyne as a free-standing electrode displaying ultra-stable and extraordinary high Li storage performance. *Energy Environ. Sci.* **2018**, *11*, 2893−2903.
(38) Wang, N.; He, J.; Tu, Z.; Yang, Z.; Zhao, F.; Li, X.; Huang, C.; Wang, K.; Jiu, T.; Yi, Y.; Li, Y. Synthesis of Chlorine-Substituted Graphdiyne and Applications for Lithium-Ion Storage. *Angew. Chem., Int. Ed.* **2017**, *56*, 10740−10745.
(39) Li, G.; Li, Y.; Liu, H.; Guo, Y.; Li, Y.; Zhu, D. Architecture of graphdiyne nanoscale films. *Chem. Commun.* **2010**, *46*, 3256−8.
(40) Jia, Y.; Zhang, L.; Du, A.; Gao, G.; Chen, J.; Yan, X.; Brown, C. L.; Yao, X. Defect Graphene as a Trifunctional Catalyst for Electrochemical Reactions. *Adv. Mater.* **2016**, *28*, 9532−9538.
(41) Zhang, S.; Du, H.; He, J.; Huang, C.; Liu, H.; Cui, G.; Li, Y. Nitrogen-Doped Graphdiyne Applied for Lithium-Ion Storage. *ACS Appl. Mater. Interfaces* **2016**, *8*, 8467−73.
(42) Ferrari, A. C.; Meyer, J. C.; Scardaci, V.; Casiraghi, C.; Lazzeri, M.; Mauri, F.; Piscanec, S.; Jiang, D.; Novoselov, K. S.; Roth, S.; Geim, A. K. Raman spectrum of graphene and graphene layers. *Phys. Rev. Lett.* **2006**, *97*, 187401.
(43) Zhong, J.; Wang, J.; Zhou, J.-G.; Mao, B.-H.; Liu, C.-H.; Liu, H.-B.; Li, Y.-L.; Sham, T.-K.; Sun, X.-H.; Wang, S.-D. Electronic Structure of Graphdiyne Probed by X-ray Absorption Spectroscopy and Scanning Transmission X-ray Microscopy. *J. Phys. Chem. C* **2013**, *117*, 5931−5936.
(44) Comelli, G.; Stöhr, J.; Robinson, C. J.; Jark, W. Structural studies of argon-sputtered amorphous carbon films by means of extended x-ray-absorption fine structure. *Phys. Rev. B: Condens. Matter Mater. Phys.* **1988**, *38*, 7511−7519.
(45) Mitsumoto, R.; Araki, T.; Ito, E.; Ouchi, Y.; Seki, K.; Kikuchi, K.; Achiba, Y.; Kurosaki, H.; Sonoda, T.; Kobayashi, H.; Boltalina, O. V.; Pavlovich, V. K.; Sidorov, L. N.; Hattori, Y.; Liu, N.; Yajima, S.; Kawasaki, S.; Okino, F.; Touhara, H. Electronic Structures and Chemical Bonding of Fluorinated Fullerenes Studied by NEXAFS, UPS, and Vacuum-UV Absorption Spectroscopies. *J. Phys. Chem. A* **1998**, *102*, 552−560.
(46) Zhou, J.; Gao, X.; Liu, R.; Xie, Z.; Yang, J.; Zhang, S.; Zhang, G.; Liu, H.; Li, Y.; Zhang, J.; Liu, Z. Synthesis of Graphdiyne Nanowalls Using Acetylenic Coupling Reaction. *J. Am. Chem. Soc.* **2015**, *137*, 7596−7599.
(47) Chen, J.; Zhang, W.; Sun, Y.; Zheng, Y.; Tang, N.; Du, Y. Creation of localized spins in graphene by ring-opening of epoxy derived hydroxyl. *Sci. Rep.* **2016**, *6*, 26862.
(48) Kogan, E. RKKY interaction in graphene. *Phys. Rev. B: Condens. Matter Mater. Phys.* **2011**, *84*, 115119.
(49) Szałowski, K. RKKY coupling between impurity spins in graphene nanoflakes. *Phys. Rev. B: Condens. Matter Mater. Phys.* **2011**, *84*, 205409.
(50) Sousa, F. J.; Amorim, B.; Castro, E. V. Dilute magnetism in graphene. *arXiv.org*, 2019, arXiv:1901.08614. https://arxiv.org/abs/1901.08614.
(51) Sang, Y.; Zhao, Z.; Zhao, M.; Hao, P.; Leng, Y.; Liu, H. From UV to Near-Infrared, WS2Nanosheet: A Novel Photocatalyst for Full Solar Light Spectrum Photodegradation. *Adv. Mater.* **2015**, *27*, 363−369.
(52) Zhang, M.-J.; Wang, N.; Pang, S.-P.; Lv, Q.; Huang, C.-S.; Zhou, Z.-M.; Ji, F.-X. Carrier Transport Improvement of CH3NH3PbI3 Film by Methylamine Gas Treatment. *ACS Appl. Mater. Interfaces* **2016**, *8*, 31413−31418.
(53) Peter, L. M.; Riley, D. J.; Tull, E. J.; Wijayantha, K. G. U. Photosensitization of nanocrystalline TiO2 by self-assembled layers of CdS quantum dots. *Chem. Commun.* **2002**, 1030−1031.
(54) Zhang, M.; Wang, X.; Sun, H.; Yu, J.; Wang, N.; Long, Y.; Huang, C. Preparation of room-temperature ferromagnetic semiconductor based on graphdiyne-transition metal hybrid. *2D Mater.* **2018**, *5*, No. 035039.
(55) Xue, Y.; Huang, B.; Yi, Y.; Guo, Y.; Zuo, Z.; Li, Y.; Jia, Z.; Liu, H.; Li, Y. Anchoring zero valence single atoms of nickel and iron on graphdiyne for hydrogen evolution. *Nat. Commun.* **2018**, *9*, 1460.
(56) Hui, L.; Xue, Y.; Huang, B.; Yu, H.; Zhang, C.; Zhang, D.; Jia, D.; Zhao, Y.; Li, Y.; Liu, H.; Li, Y. Overall water splitting by graphdiyne-exfoliated and -sandwiched layered double-hydroxide nanosheet arrays. *Nat. Commun.* **2018**, *9*, 5309.
(57) Hui, L.; Xue, Y.; Yu, H.; Liu, Y.; Fang, Y.; Xing, C.; Huang, B.; Li, Y. Highly Efficient and Selective Generation of Ammonia and Hydrogen on a Graphdiyne-Based Catalyst. *J. Am. Chem. Soc.* **2019**, *141*, 10677−10683.
(58) Yang, S.; Li, W.; Ye, C.; Wang, G.; Tian, H.; Zhu, C.; He, P.; Ding, G.; Xie, X.; Liu, Y.; Lifshitz, Y.; Lee, S. T.; Kang, Z.; Jiang, M. C3 N-A 2D Crystalline, Hole-Free, Tunable-Narrow-Bandgap Semiconductor with Ferromagnetic Properties. *Adv. Mater.* **2017**, *29*, 1605625.
(59) Li, Y.; Zhang, M.; Hu, X.; Fan, X.; Yu, L.; Huang, C. Light and Heat Triggering Modulation of the Electronic Performance of a Graphdiyne-Based Thin Film Transistor. *J. Phys. Chem. Lett.* **2020**, *11*, 1998−2005.

https://dx.doi.org/10.1021/acscentsci.0c00348
ACS Cent. Sci. 2020, 6, 950−958